Surface Forces in Solutions Containing Rigid Polymers: Approaching the Rod Limit

Jan Forsman*

Theoretical Chemistry, Chemical Centre, P.O. Box 124, S-221 00 Lund, Sweden

Clifford E. Woodward

School of Physical Environmental and Mathematical Sciences, University College, University of New South Wales, Building 22, Australian Defence Force Academy, Canberra ACT 2600, Australia

Received November 18, 2005

ABSTRACT: In a recent paper,[1] we investigated how the interaction between two adsorbing surfaces in a polymer solution responds to changes of the intrinsic stiffness of the polymer chains. We demonstrated that as the chain rigidity is increased, starting from the fully flexible limit, a free energy barrier develops. In this work, we shall continue our studies of semiflexible polymers but focus on the other extreme, where the stiffness is increased to the extent that the chains become rodlike. In this limit, the free energy barrier disappears and is replaced by a long-ranged attraction. A weak barrier at separations corresponding to the length of a fully stretched chain is, however, present. The approach to rodlike behavior is very slow at low polymer concentrations; i.e., rods will under these conditions behave in a manner which is qualitatively different from that of even extremely rigid semiflexible chains. At higher concentration, a slightly different picture emerges, since saturation effects will prevent an exceptionally strong adsorption of rods. Semiflexible polymers will then display reasonably "rodlike" behavior at a more moderate chain rigidity. Still, our results suggest that models of semiflexible chains as rods or cylinders should be treated with considerable caution, at least in terms of adsorption or surface force properties. Our results furthermore show that the results for explicit solvent models, adopted in our previous work, are in this case qualitatively reproduced by simpler models, where the solvent enters implicitly. The agreement across a range of different model systems, of which some are solved exactly, lends support to the qualitative conclusions drawn from our studies on these systems. Finally, we compare structural density functional predictions with corresponding simulation results. The predictions are accurate, except in the case of extremely stiff chains and rodlike chains. These display considerable ordering at the surfaces, a phenomenon that cannot be captured by the present density functional. This leads to a significant underestimation of the primary adsorption peak. However, comparisons between surface forces in rod solutions, as obtained from grand canonical simulations and density functional calculations, demonstrate that the ordering transitions have little influence on the surface interactions. This is because the surface interactions are governed by the free chains, which are not strongly adsorbed to any surface. We also show that the small quantitative effect that surface ordering does have on the surface forces, in principle, can be handled in an effective manner by a simple increase of the surface potential strength.

1. Introduction

Polymers are in general not completely flexible but contain some degree of internal stiffness. The origin of this stiffness can be due to, for example, steric constraints, multiple covalent bonding, or charge repulsion. Stiff polymers are sometimes described theoretically as rodlike molecules. The removal of intrinsic degrees of freedom leads to a much simpler model. Several theoretical and experimental studies on rodlike polymers and colloids[2−11] have demonstrated that rods have interesting properties, with the potential for practical applications in the area of colloid and polymer science. Few studies have been devoted to the study of polymers which, though very stiff, are not rods. This work will help establish when the rodlike limit is a valid model of very stiff chains.

Recently, Lau et al.[12] used a very simple model of a "bent" rod, composed of two linear rods at a fixed angle. Their findings imply that the rod model may not be a satisfactory one, even for very stiff chains, although it is not clear how well their simplified model is able to reproduce properties of very stiff polymer molecules.

* Corresponding author. E-mail: jan.forsman@teokem.lu.se.

We shall extend the density functional studies in our previous work[1] on semiflexible polymers to cases where the persistence length exceeds the chain length. Indeed, we shall also treat the limiting case of rods themselves. Our focus will be on forces between adsorbing surfaces at full equilibrium (complete bulk exchange). The monomers are connected with bonds of fixed length, and the chain stiffness is regulated via a bond angle potential, which effectively amounts to a repulsion between next-nearest neighbors along the chain. To facilitate studies of the rod limit,[13] we shall restrict the study to rather short polymers, usually 30-mers.

Another difference between this work and our previous one on semiflexible chains[1] is that here we will employ implicit solvent models. There are two reasons for this. Since the chains are short, their influence on surface forces is restricted to a rather short range, where the results would be obscured by solvent packing effects, were the solvent particles treated explicitly. In addition, it is of interest to at least qualitatively compare predictions obtained with explicit and implicit solvent approaches. Our previous studies[14−16] have demonstrated that in some systems there are qualitative differences between the predictions of implicit and explicit solvent models. We will show

10.1021/ma052472+ CCC: $33.50
Published on Web 01/04/2006

that for the systems we study here the different model approaches do agree qualitatively. The exactly solvable ideal semiflexible (and rodlike) polymer fluid will serve as a useful reference system.

The predictive powers of the density functional theories will be evaluated by explicit structural comparisons with simulation results.

1.1. Theory and Model Description. *1.1.1. Model Review.* We start by a brief review of the model system and the general structure of the density functional theory. Connected monomers are separated by a fixed bond distance σ, which, in the case of nonideal polymer fluids, also defines the monomer hard-sphere diameter. A configuration of an r-mer is represented by $\mathbf{R} = (\mathbf{r}_1, ..., \mathbf{r}_r)$, where $\mathbf{r}_i$ is the coordinate of monomer i. The free energy functional for ideal chains is exactly given by[17]

$$\beta\mathscr{F}_p^{id}[N(\mathbf{R})] = \int N(\mathbf{R})(\ln[N(\mathbf{R})] - 1)\, d\mathbf{R} + \beta\int N(\mathbf{R})\, V_b(\mathbf{R})\, d\mathbf{R} \quad (1)$$

where β is the inverse thermal energy and $N(\mathbf{R})$ is a polymer density distribution, defined such that $N(\mathbf{R})\, d\mathbf{R}$ is the number of polymer molecules having configurations between $\mathbf{R}$ and $\mathbf{R} + d\mathbf{R}$. Adjacent monomers in a chain are connected by a bond potential $V_b(N(\mathbf{R}))$, which has no angular component but is infinitely rigid in the sense that it ensures that the bond distance is fixed at σ. The monomer density, $n_m(\mathbf{r})$, is given by $n_m(\mathbf{r}) = \int_{i=1}^{r}\delta(\mathbf{r} - \mathbf{r}_i)N(\mathbf{R})\, d\mathbf{R}$. Hard-core interactions are approximated by an excess free energy term, $\mathscr{F}^{ex}[\bar{n}_m(\mathbf{r})]$, which in this paper is a functional of the monomer density only. An explicit expression for this has been provided elsewhere.[18] The grand potential of an athermal polymer fluid, in the presence of an external potential $V^{ext}(\mathbf{r})$, can thus be written as

$$\beta\Omega[N(\mathbf{R})] = \beta\mathscr{F}_p^{id}[N(\mathbf{R})] + \beta\mathscr{F}^{ex}[\bar{n}_m(\mathbf{r})] + \int\beta(V_m^{ext}(\mathbf{r}) - \mu_p)n_m(\mathbf{r})\, d\mathbf{r} \quad (2)$$

where μ_p is the polymer chemical potential. The free energy per unit area, g_s, is given by $g_s = \Omega_{eq}/S + P_b h$, where Ω_{eq} is the equilibrium grand potential, P_b is the bulk pressure, and S is the surface area. g_s will at large separations approach twice the interfacial tension of the fluid at a single wall, γ_w. Hence, the net solvation free energy is obtained from: $\Delta g_s = g_s - 2\gamma_w$. The solvation pressure, P_s, can be calculated from $P_s = -\partial g_s/\partial h$ or via a virial expression.

Polymer rigidity is modulated by a bond angle potential, E_b, between next-nearest neighbors along a chain. Specifically

$$\beta E_b = \epsilon\left(1 - \frac{\mathbf{s}_i\mathbf{s}_{i+1}}{\sigma^2}\right) \quad (3)$$

where $\mathbf{s}_i$ denote the bond vector between monomers i and $i + 1$, and ϵ is the parameter we use to modulate the intrinsic stiffness of the polymer. The way in which this stiffness potential is incorporated into a density functional theory of semiflexible polymer solutions has been described previously[1,18] and will not be repeated here. The persistence length, $\lambda_p = \langle\mathbf{R}_{ee}\mathbf{s}_1/\sigma\rangle$, is given by

$$\lambda_p/\sigma = \frac{\epsilon(1 - e^{-2\epsilon})}{1 - e^{-2\epsilon}(1 + 2\epsilon)} \quad (4)$$

which in practice means that in most cases, $\lambda_p/\sigma \approx \epsilon$.

1.1.2. Rods. The extension of the density functional theory to treat the case where the monomers are connected to form a rod is straightforward. The ideal part of the free energy functional, $\mathscr{F}_{pi}^{d}$, will have the same appearance as in eq 1, although the number of possible polymer configurations naturally is strongly reduced by the rod constraint. The expression for the equilibrium profile of monomers connected to form a truly rodlike chain, in a slit where the surfaces are separated a distance h, is given by

$$n_m(z) = \sum_{k=1}^{r}\int_{\max[0,\, z-(r-k)\sigma,z-k\sigma]}^{\min[h,z+(r-k)\sigma,z+k\sigma]}\prod_{i=1}^{r} e^{(\beta\mu_p - \lambda_m(z+(i-k)\sigma\cos\theta))}\, d\cos\theta \quad (5)$$

where $\lambda_m(z) = \partial\beta F_{ex}/\partial n_m(z)$ is the mean field at position z from the left wall. Note that we have integrated out the x, y dimensions, with a mean-field approach. Hence, while this functional is the appropriate infinite-stiff correspondence to the one we have used for semiflexible chains, it is unable to describe smectic-like ordering. This flaw has some consequences for the quantitative accuracy with which the functional predicts adsorption properties. However, we will demonstrate that the occurrence of smectic ordering has very little influence on the surface interactions, which is our focus in this study.

1.1.3. Implicit Solvent Models. As mentioned above, the solvent is treated implicitly in this work, which means that the pressures acting on the surfaces should be regarded as osmotic pressures. We shall use two different models, which we denote as the "polymer fluid" and the "incompressible fluid" models. The first simply amounts to treating the solution as a low-density polymer melt. This model can in principle be mapped to a corresponding polymer solution, using McMillan−Mayer theory.[19] We will not describe this here, but it should be noted that if the fluid is approximated as being incompressible, the Gibbs−Duhem relation between the osmotic pressure and the chemical potential of the solvent becomes very simple. The "incompressible fluid" approach, which essentially is a continuum version of the Scheutjens−Fleer theory,[20] was introduced in an earlier study.[15] The main assumption is a local incompressibility constraint for the solution, i.e., $n_s(z) + n_m(z) = n_0$, where n_0 is the fixed total density. Substituting this into the expression for the grand potential, eq 2, we get

$$\beta\Omega[N(\mathbf{R}),n_m(z)] = \beta\mathscr{F}_p^{id}[N(\mathbf{R})] + \int\{n_0 - n_m(z)\}\{\ln[n_0 - n_m(z)] - 1\}\, dz + \beta\mathscr{F}^{ex} + \int\beta\{V_m^{ext}(z) - \mu_p\}n_m(z)\, dz + \int\beta\{V_s^{ext}(z) - \mu_s\}\{n_0 - n_m(z)\}\, dz \quad (6)$$

where $\mathscr{F}^{ex}$ is a functional of the local total density and μ_s is the chemical potential of the solvent. The total density is constrained to be constant, which means that $\mathscr{F}^{ex}$ is a constant. Hence, the free energy can be considered a functional of the monomer density only and thus describes an effective one-component polymer fluid. Note that, given the incompressibility approximation and the neglect of intramolecular correlations other than via the bonding and stiffness potentials (mean-field assumption), the results obtained with this functional are exact. In other words, the approach does not rely on the use of an approximate equation of state.

1.1.4. Midplane Pressure Contributions. Further insight into the mechanisms underlying the net surface interactions in the system can be obtained by analyzing the separate contributions, across the midplane of the slit, to the osmotic pressure acting

perpendicular to the walls. The formal expressions for these has been provided previously.[1,21] We will here only provide a description of their physical significance. The midplane contributions are (i) a repulsive ideal entropic pressure, P_{en}, given by the total particle density at the midplane, (ii) a repulsive pressure, P_{coll}, due to collisions between particles on either side of the midplane, (iii) an attractive pressure, P_{acr}, from particles on one-half of the midplane interacting with the surface on the other side, and (iv) an attractive pressure, P_{bridge}, generated by chains crossing the midplane. Since most of these contributions are large in magnitude and have separate signs, it is useful to consider their respective change relative to their value in the bulk. These "excess" quantities will be denoted ΔP_{en}, etc.

1.1.5. Surface Potentials. The same type of surface potential as used in our previous studies[1,15,21] will be used for the implicit solvent models. However, if solvent and monomer particles were to be equally attracted to the surfaces in the incompressible fluid description, monomers would not experience *any* net attraction to the surfaces. This would result in polymer depletion, as described in ref 15. To model surfaces that attract polymers in this model system, it is necessary to adopt a discriminating adsorption potential. Specifically, in the incompressible fluid and polymer fluid approaches, the following surface potential will be adopted:

$$w(z) = A_w e^{-z/\sigma} w_{L-J}(z) \tag{7}$$

acting on the *monomers* only. We set $A_w \approx 2.7057$, in accordance with our previous work.[15] $w_{L-J}(z)$ is a Lennard-Jones wall interaction, $\beta w_{L-J}(z) = 2\pi[2/45\,(\sigma/z)^9 - 1/3\,(\sigma/z)^3]$. Since there are two walls, the total surface interaction is given by $V_m^{ext}(h,z) = w(z) + w(h - z)$.

As it turned out, the ideal rod fluid shows an anomalously large adsorption with the above potential. This led to particularly large values for P_{acr}. P_{acr} is very small in the other systems we investigated. To obtain more comparable results, we chose to use a truncated and shifted Lennard-Jones surface interaction for the ideal fluid:

$$w^{id}(z) = 0.4(w_{L-J}(z) - w_{L-J}(z_c)) \tag{8}$$

The range was limited to $z_c = 2.2\sigma$, which makes P_{acr} identically zero for $h > 4.4\sigma$. The factor 0.4 adjusts the surface strength to achieve strong, but "reasonable", adsorption, at least for flexible, up to very stiff, chains. We stress that very similar net surface forces are obtained with both exponentially decaying (eq 7) and truncated and shifted (eq 8) surface potentials.

We have chosen to present our results in two separate sections. The first part includes density functional predictions of surface interactions in our model systems. In the second part, we will make comparisons with corresponding simulation results. These will, with one exception, be limited to structural comparisons. The surface potentials are strong enough to induce ordering at the surfaces, which cannot be captured by our present functionals. We have therefore included an explicit surface force comparison, for a hard-sphere rod fluid, under conditions where such an ordering occurs at the surfaces. This comparison clearly shows that the ordering has little influence on the surface forces, which is dominated by a depletion of free (not strongly adsorbed) rods.

2. Results

2.1. Part I. Density Functional Predictions of Surface Forces. *2.1.1. The Polymer Fluid Model.* We will first briefly have a look at structural features to demonstrate how strongly adsorbing the surfaces are for chains of different stiffness. This is shown in Figure 1. We note that the rods display an adsorption that by far exceeds even that of the most rigid chains investigated. It should be pointed out that although the rods adsorb very strongly at the surfaces, the monomer profile has a depleted form in the central portion of the slit. This cannot be detected on the scales of Figure 1 but will be explicitly presented and further discussed below. The adsorption is very strong in these cases. However, we have confirmed (not shown) that more moderately adsorbing walls lead to surface forces with the same qualitative behavior.

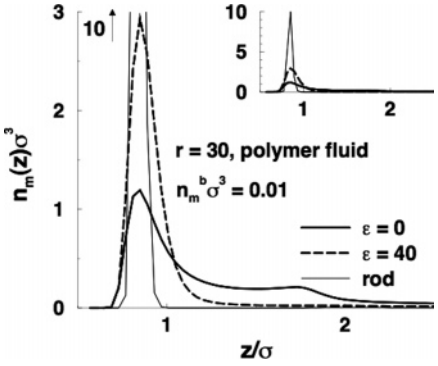

Figure 1. Monomer density profiles between surfaces separated by 40σ, where σ is the bond length as well as the diameter of the hard-sphere monomers. Profiles for fluids with chains of various rigidity, as regulated by the stiffness parameter ϵ, are given. The arrow, shouldered by the number 10, indicates that the curve has been truncated and that it peaks at a value of about 10. The inset shows the full adsorption peak obtained for the rod fluid. In all cases, the 30-mer fluids are in equilibrium with a bulk, in which the monomer density is $n_m^b\sigma^3 = 0.01$.

Let us now study the surface forces of the system. We noted in our previous work on polymer solutions with explicit solvent representation[16] that, as the intrinsic stiffness is increased from the fully flexible limit, the surface interaction displays a free energy barrier at intermediate separations. If the chains are even more rigid, a significant minimum appears outside this barrier. When the monomer concentration is high, this minimum has already developed for moderately stiff polymers. In Figure 2, we can see that this overall behavior is predicted also with the polymer fluid approach. We have investigated two different monomer concentrations: $n_m^b\sigma^3 = 0.01$ and 0.1. As the rod limit is approached, the barrier at intermediate separations gradually weakens and finally disappears. Instead, a new barrier is developed at separations corresponding to the fully stretched chain, i.e., one rod length. At low monomer concentrations, this barrier at long range is weak. In fact, it is undetectable on the scale displayed in Figure 2a. At higher concentrations the barrier is significant and increases with chain rigidity.

Rodlike behavior of the force curves is approached more rapidly (with ϵ) when the monomer concentration is higher. We interpret this as a saturation effect. The exceptionally strong adsorption of rods renders the surfaces essentially saturated with monomers, at both low and high bulk monomer concentrations. Semiflexible chains do not adsorb as strongly and do not saturate the surfaces at low monomer concentrations, unless the chain rigidity is exceptionally high. However, when the bulk density is high, surface saturation is reached for a more moderate polymer stiffness, which leads to force curves resembling that of the corresponding rod solution.

We can obtain further insight by analyzing the midplane pressure contributions. Figure 3 shows entropic and bridging

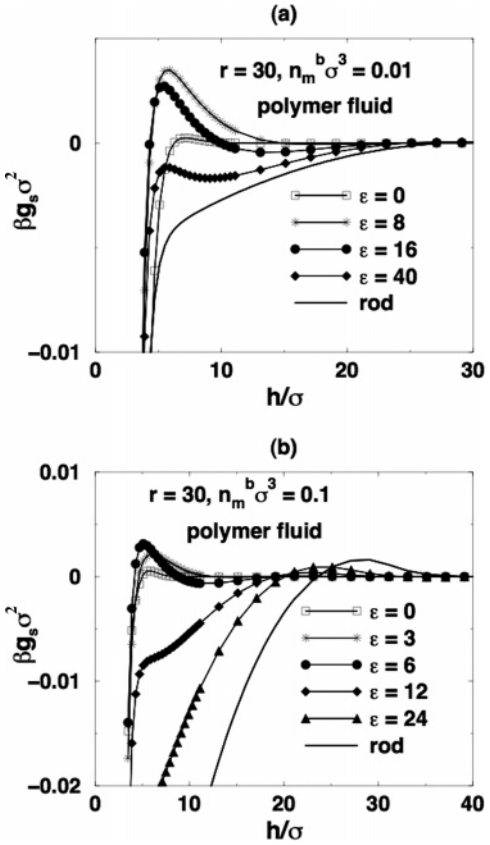

Figure 2. Influence of intrinsic chain stiffness on surface interaction free energies in 30-mer solutions, as predicted by the polymer fluid approach, at two different bulk monomer densities: (a) $n_m^b\sigma^3 = 0.01$; (b) $n_m^b\sigma^3 = 0.1$.

pressure contributions at the midplane for the dilute and concentrated polymer solutions.

Let us discuss the following cases separately:

• Low concentration, moderate stiffness ($n_m^b\sigma^3 = 0.01$, $\epsilon = 0, 8$): there is a weak depletion at moderate to large separations. This is caused by expulsion of polymer molecules, which are not strongly adsorbed to the surfaces, due to the entropically restrictive environment of the surfaces. At shorter separations, the contribution to the free energy comes mainly from the overlap of the coronal region of the adsorbed polymers, made up of tails and loops. The overlap of these regions as the surfaces approach one another leads to an increase in the midplane monomer density. However, these polymers do not bridge strongly, and there is a relatively slow growth in the bridging contribution. Thus, the free energy becomes repulsive. At even closer separations, the polymer molecules are able to bridge substantially and the free energy becomes attractive, leading to the formation of a barrier. The separation at the barrier's maximum is about $h/\sigma = 5$ and seems to be independent of stiffness. Thus, it does not scale with persistence length, appearing instead to be a function of local monomer structure.

• Low concentration, high stiffness ($n_m^b\sigma^3 = 0.01$, $\epsilon = 40$, rods): now, the depletion regime extends down to much shorter separations, resulting in a substantial depletion attraction. This is related to the adsorption profile becoming sharper for stiffer chains, as these have an extremely low propensity to project out into the solution. Hence, overlap of the adsorption profiles, with a concomitant increase of the mid plane density, only occurs at very short separations, for stiff chains. Moreover, stiff chains that are not strongly adsorbed will sense the entropic restriction by the surfaces at relatively large distances. This leads to a long-ranged depletion attraction. A tiny barrier, close to $h/\sigma = 30$, occurs for rods, while the solution containing very stiff polymers still shows some remnant of the barrier at short range. At short separations, bridging again dominates and the free energy there is attractive. The rod solution displays rapid oscillations of ΔP_{en} and ΔP_{br} at these separations. These oscillations are anticorrelated and essentially cancel out; i.e., they do not give rise to dramatic changes of the interaction free energy.

• High concentration, moderate stiffness ($n_m^b\sigma^3 = 0.1$, $\epsilon = 0$, 6): the behavior is qualitatively similar to what we observed at low concentrations, although the regime in which ΔP_{en} is net repulsive now has a much shorter range.

• High concentration, high stiffness ($n_m^b\sigma^3 = 0.1$, $\epsilon = 24$, rods): again, the rod solution generates ΔP_{en} and ΔP_{br} which are rapidly varying at short range. However, since this provides little insight and tends to obscure the relevant information in the graph, we do not show the short-range part of the rod curves. At this higher density, the wide depletion regime we see for the rod fluid, extending from short to large separations, is already present for $\epsilon = 24$. This confirms the conclusion that rodlike behavior in the surface interactions is more rapidly approached at high concentrations.

2.1.2. The Incompressible Fluid Model. We also investigated the predictions of the incompressible fluid model. The total fluid density is constrained to the value for a simple cubic lattice: $n_0\sigma^3 = 1$.

Monomer density profiles are given in Figure 4. We see that the limits on allowed local density variations, imposed by the incompressibility constraint, has a dramatic effect on appearance of these profiles (cf. the polymer fluid model). The adsorption is forced to be moderate for the rod fluid as well.

The incompressibility constraint also influences the surface interactions, but essentially only in a quantitative manner. The resemblance of the surface interaction curves, presented in Figure 5, to those obtained with the polymer fluid approximation (cf. Figure 2) is remarkable, given the difference between the corresponding adsorption profiles. The absolute magnitude of the surface interactions in the incompressibility model is much weaker. Nevertheless, it is encouraging to find the same qualitative behavior with quite different models. The qualitative features of the surface forces, and the response of the surface interaction to changes of the bulk concentration and the chain stiffness, were discussed in the previous section, and we shall not repeat the arguments here.

2.1.3. Ideal Polymers. As discussed earlier, for ideal polymers, we have used a short-ranged surface potential. We stress, however, that all qualitative features of the results presented are retained if an adsorption potential of the type used above (cf. eq 7) is used.

A surface that attracts monomers strongly enough to generate a positive adsorption for a fully flexible ideal chain will produce an enormously strong adsorption for ideal rods. This is demonstrated in Figure 7. We see that even if the ideal polymers are *extremely* stiff, with a persistence length ($\approx\epsilon\sigma$) far exceeding the fully stretched chain, they are not nearly as attracted to the surfaces as are rods. This is of course partly due to the lack of saturation effects, but we found similar adsorption differences (though smaller in magnitude) also with the polymer fluid approximation. The inset of the graph clearly illustrates that rods, even when they adsorb exceptionally strongly, still has a depleted behavior some distance away from the walls, extending all the way to the midplane. This is why we obtain the paradoxical behavior of a long-ranged depletion attraction

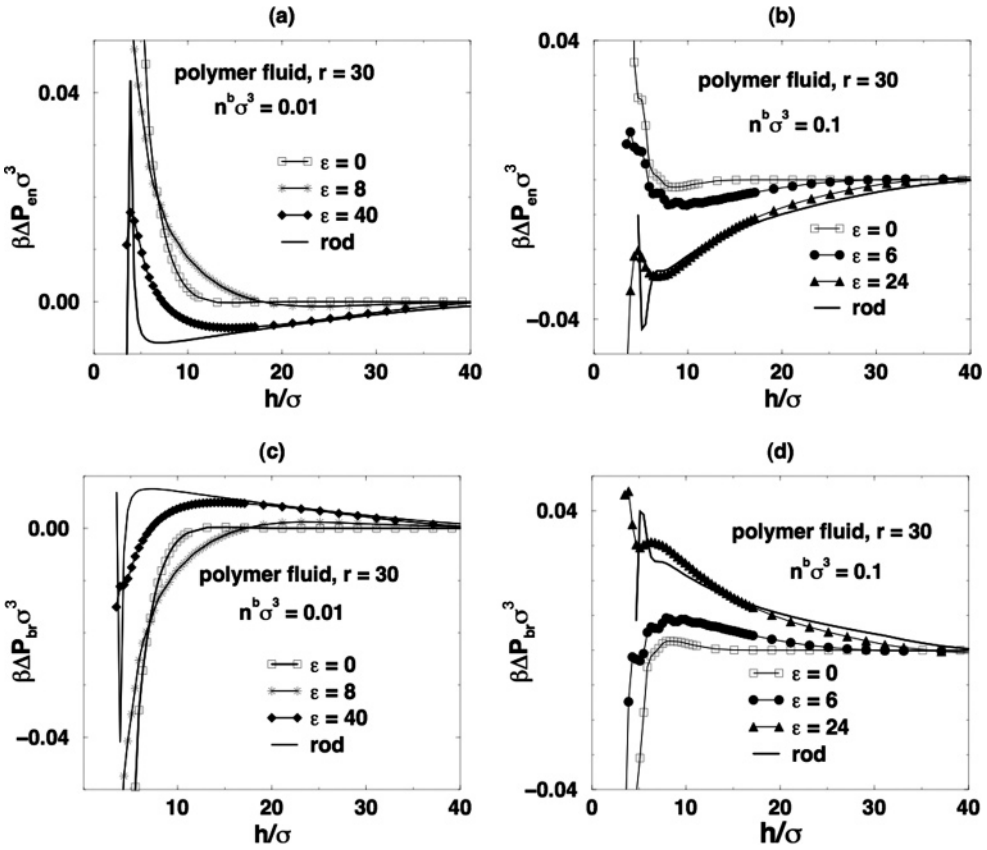

Figure 3. Entropic, P_{en}, and bridging, P_{br}, pressure contributions at the midplane for the surface interactions given in Figure 2. For visual reasons, some curves are absent. Note that excess quantities are shown, i.e., $\Delta P_{en}(h) = P_{en}(h) - P_{en}^b$, where P_{en}^b is the entropic pressure in the bulk. (a) ΔP_{en}, $n_m^b\sigma^3 = 0.01$; (b) ΔP_{en}, $n_m^b\sigma^3 = 0.1$; (c) ΔP_{br}, $n_m^b\sigma^3 = 0.01$; (d) ΔP_{br}, $n_m^b\sigma^3 = 0.1$.

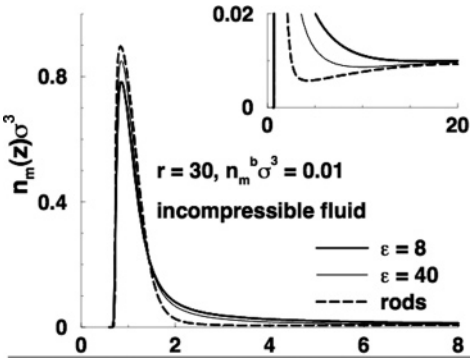

Figure 4. Monomer density profiles for 30-mers, as obtained with the incompressible fluid approximation, for different degrees of chain rigidity. The surface separation is 40σ, and the bulk monomer density is $n_m^b\sigma^3 = 0.01$. Th inset is a blow-up, showing how the density is depleted some distance away from the walls, when the chains are very rigid.

between strongly adsorbing surfaces. The reason for the depletion is that rods which are not strongly adsorbed will be entropically restricted in the slit, even at rather large separations. Interestingly, the vast differences we observe for the adsorption profiles are not really reflected in the surface forces. Still, the rod fluid produces a monotonic attraction, while even the stiffest semiflexible chain fluid has a free energy barrier at short range. This is similar to our observations at low bulk monomer density with the polymer fluid as well as the incompressible solvent model. This is not unexpected since those approximations should approach the predictions for ideal chains for vanishing bulk concentrations. Finally, we present the separate pressure contributions across the midplane for the ideal polymer fluids. Again, we expect results qualitatively similar to those obtained with the polymer fluid approach, at low concentrations (cf. parts a and c of Figure 3). It is nevertheless of interest to establish these quantities for a model that can be solved exactly. The results are given in Figure 8, and they confirm our conjecture. We see that the attraction at long range is caused by depletion, while the barrier found at short range for semiflexible polymers is due to accumulation in combination with relatively weak bridging forces. It is interesting to note how the magnitude of the separate contributions (even only their excess part) by far exceeds the net pressure (cf. Figure 7). In other words, the net osmotic pressure is the result of an almost complete cancellation between very large, but opposite, contributions across the midplane. This is a general observation, also valid for polymer fluid and polymer solution models. Note also how the decay of the entropic and bridging contributions to their respective bulk values is remarkably slow, in particular for the more rigid chains.

2.2. Part II. Comparisons with Simulation Results. In the following, density functional results will often be denoted by "DFT". Analogously, "MC" stands for canonical Monte Carlo simulations, while "GCMC" indicates that the simulations were performed by a grand canonical scheme.

2.2.1. Structural Comparisons of Semiflexible Polymer Fluids. The structure of confined semiflexible polymer fluids, as predicted by density functional calculations, will be compared with corresponding results from canonical simulations. It would have been of greater interest to establish the accuracy of surface force predictions instead. However, surface interactions (at full particle equilibrium) are very expensive to obtain from simulations. Several different simulation methods have been developed to deal with the bulk exchange criteria in efficient ways.[22−29] Such simulations are nevertheless computationally demanding,

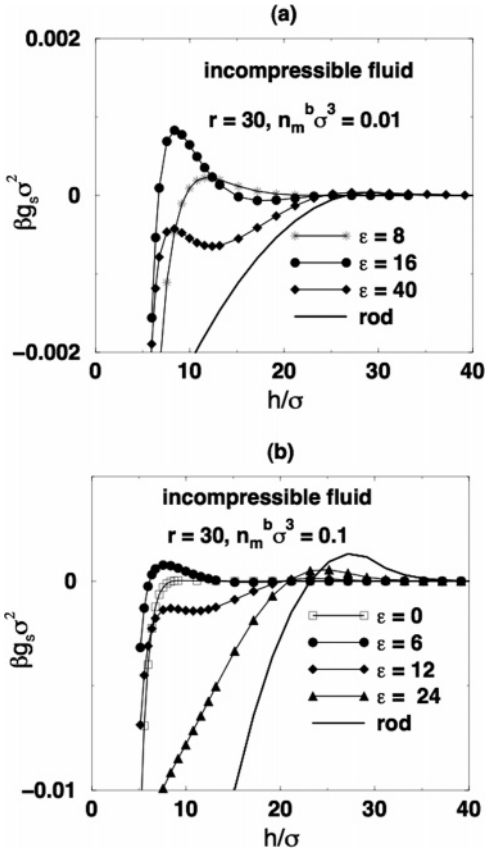

Figure 5. Influence of intrinsic chain stiffness on surface interaction free energies, as predicted by the incompressible fluid approach, at two different bulk monomer densities. The total density of the incompressible fluid is constrained to be $n_0\sigma^3 = 1$. (a) $n_m^b\sigma^3 = 0.01$; (b) $n_m^b\sigma^3 = 0.1$.

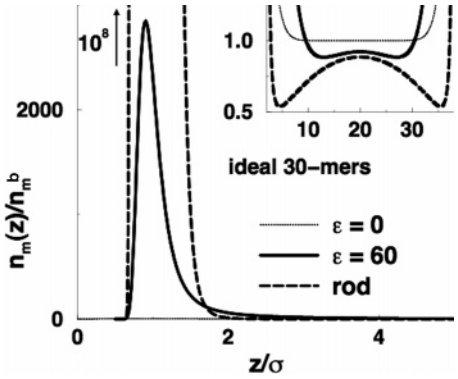

Figure 6. Monomer density profiles for ideal 30-mers in a slit with surface separation $h/\sigma = 40$. The solid line shows the adsorption of chains are in principle semiflexible, but extremely stiff: $\epsilon = 60$. The thick dashed line is the solution in the true rod limit, i.e., "30-mer rods". The thin dotted line is included as a reference. It gives the adsorption profile for the other extreme: completely flexible polymers. The note in the upper left of the graph indicates that the rod profile peaks at about $n_m(z)/n_m^b = 10^8$. The inset is a blow-up of the central portion of the profile. Here we see that there is indeed a positive adsorption of the flexible molecules, although it is too weak to be detected on the large scale. Stiff chains display a qualitatively different behavior from flexible ones, with a depleted profile in the central portion of the slit. Note that a truncated and shifted potential has been used for the ideal fluids; see eq 8.

and we have not implemented them in this work. We will, however, report such results in the near future. It should be noted that a recent work on flexible short chain fluids,[30] with monomers connected by harmonic springs, did focus on the ability of a density functional theory to predict interactions

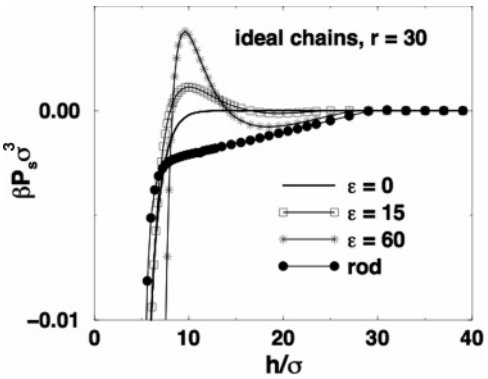

Figure 7. Influence of intrinsic chain stiffness on net solvation pressures, in ideal 30-mer polymer fluids. The bulk monomer density is $n_m^b\sigma^3 = 0.1$.

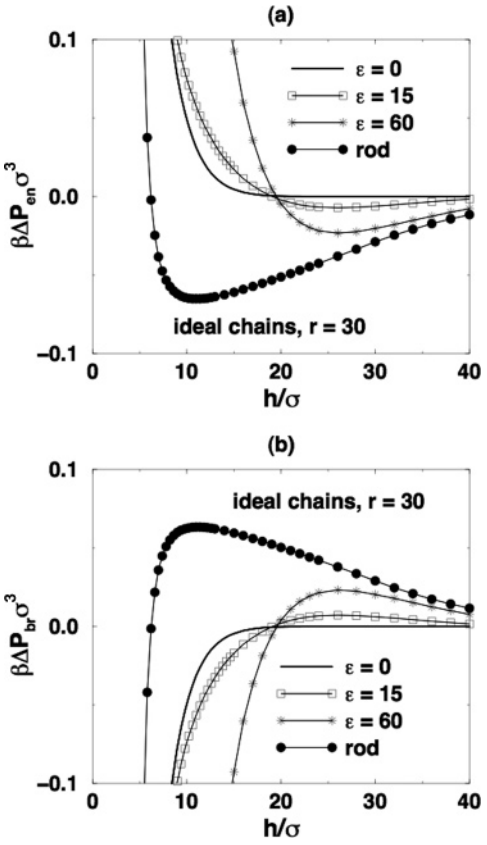

Figure 8. Entropic, ΔP_{en}, and bridging, ΔP_{br}, excess pressure contributions at the midplane for surface interactions in ideal polymer fluids. Note the difference in scale, as compared with Figure 7. (a) Entropic excess part: ΔP_{en}. (b) Bridging excess part: ΔP_{br}.

between adsorbing surfaces. The agreement was remarkable, both for fluids with repulsive and attractive monomer−monomer interactions.

We have used the same surface potential ($A_w \approx 2.7057$) and chain length ($r = 30$) as in the previous part of this paper. Average monomer densities are calculated over the allowed regions between the surfaces, i.e., outside 0.5σ from each wall. Specifically, we performed all simulations at $h = 8\sigma$ and the average monomer density is fixed at

$$\langle n_m(z)\rangle_{0.5\sigma,h-0.5\sigma} \equiv \frac{\int_{0.5\sigma}^{h-0.5\sigma} n_m(z)\,dz}{h-\sigma} = 0.15 \qquad (9)$$

There are several ways in which these results can be compared with DFT. In the DFT approach, the bulk density (or chemical

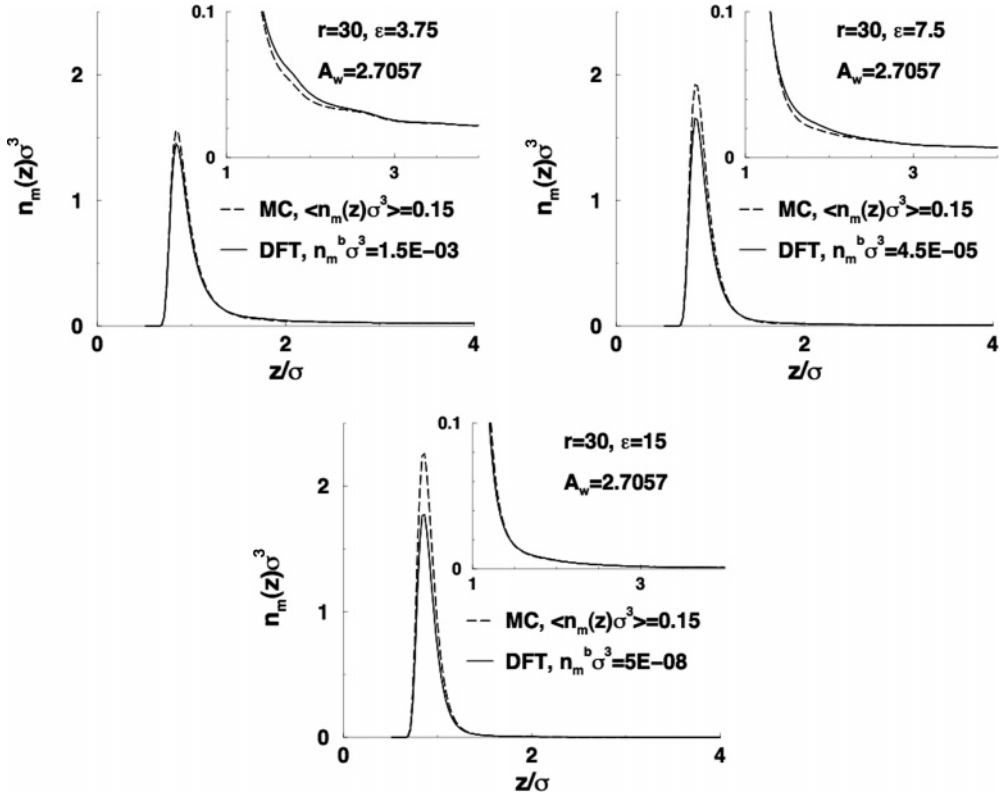

Figure 9. Monomer density distributions in athermal 30-mer fluids with different degrees of intrinsic chain stiffness, as regulated by the bond angle potential parameter ϵ. "DFT" are density functional predictions, while "MC" denotes results from canonical Metropolis Monte Carlo simulations. The simulated data have been symmetrized across the midplane to increase accuracy and precision. Low-density regimes are highlighted in the insets. The bulk conditions of the DFT calculations are chosen such that the midplane density agrees with the corresponding MC data. These bulk monomer densities are given in the legends.

potential) is the natural "input variable". Hence, one option is to adjust the bulk density until the average monomer density in the slit fulfills eq 9. However, as our paper focuses on surface interactions, it is more appropriate to adjust the bulk density until the midplane density agrees with that obtained in the simulations. This should also serve as a reasonable estimate of the corresponding bulk, had the simulations been performed in an open (grand canonical) ensemble. Hence, with this approach the comparisons between MC and DFT are made at roughly equal bulk densities.

The usual Metropolis[31] algorithm was employed, with periodic boundary conditions applied in the $x-y$ plane, parallel to the surfaces. Attempts to displace the polymer and monomer particles were made via crankshaft moves, reptations, or translations of the whole molecule. The simulations were performed in a geometry where the lateral size, L, of the simulation box was $L \approx 30.24\sigma$ (i.e., 32 chains). This ensures that we do not obtain errors due to self-interactions of rodlike chains lying flat on the surfaces.

We have compared monomer density distributions of semiflexible hard-core 30-mer fluids, with $\epsilon = 3.75$, 7.5, and 15. The results are presented in Figure 9. We see that the agreement is quite satisfactory for the fluid containing relatively flexible chains, although the theory slightly underestimates the height of the primary adsorption peak. This disagreement increases as the intrinsic stiffness becomes progressively stronger and is substantial for the stiffest polymers, with $\epsilon = 15$. This is probably related to the inability of the DFT to handle ordering at the surfaces. Such an ordering leads to a more efficient packing of the chains at the surfaces. Guided by "configuration snapshots" of the kind presented for rods below, we would in a crude manner characterize the stiffest adsorbed chains ($\epsilon = 15$) as being "ordered", while the more flexible ones ($\epsilon = 7.5$ and $\epsilon = 3.75$) are not. This is of course not a rigorous analysis, and the transition from "disordered" to "ordered" appears to be gradual. For instance, there are *some* tendencies to surface alignment when $\epsilon = 7.5$, but not very pronounced. At any rate, the occurrence of surface "ordering" manifests itself in terms of stronger adsorption, which is apparent from the remarkably small bulk concentration required in order to obtain agreement between DFT and MC at the midplane, when $\epsilon = 15$.

2.2.2. Structural and Surface Force Comparisons of Rod Fluids. As we have already noted, rods display anomalously strong adsorption. Unfortunately, this puts some limits on what conditions we can reliably simulate. On the other hand, the lack of intramolecular degrees of freedom makes rods a suitable candidate for grand canonical simulations, which in turn offers the possibility of surface force calculations.

We have therefore chosen to limit this study to 15-mer rod fluids and have also reduced the surface potential strength. Specifically, we will investigate two different choices of the surface amplitude: $A_w = 0.4$ and $A_w = 1.25$. In the latter case the system displays smectic ordering at the surfaces, but the potential is still weak enough to permit reliable estimates of surface forces. The former potential is too weak to induce surface ordering, and we shall see that this has a large influence on the *structural* agreement between simulated data and DFT predictions.

As mentioned, the simulation of rods will be performed in the grand canonical ensemble (GCMC). These were performed in the same standard manner as described above, although crankshaft moves were replaced by molecule rotations. The lateral size of the simulation box was fixed at $L = 23\sigma$.

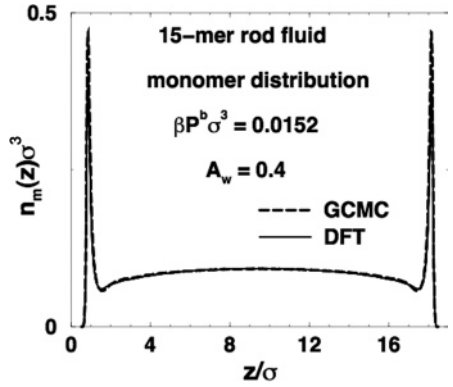

Figure 10. Predicted and simulated monomer density distributions in athermal fluids of rodlike 15-mers between weakly attractive surfaces: $A_w = 0.4$. The surface separation is $h = 19\sigma$. This system does not display significant surface ordering.

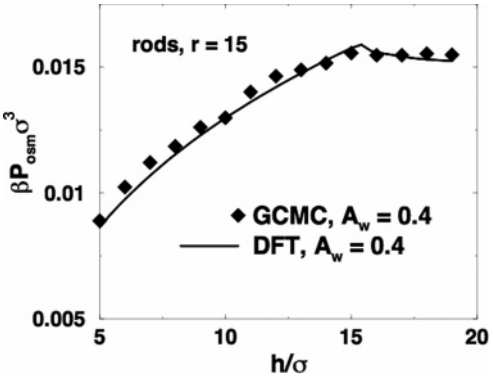

Figure 11. Predicted and simulated osmotic pressure curves in athermal fluids of rodlike 15-mers between weakly attractive surfaces: $A_w = 0.4$. The osmotic pressure, P_{osm} is the sum of the net solvation pressure and the bulk pressure: $P_{osm} = P_s + P^b$.

We start by showing that the functional is able to predict adsorption characteristics as well as surface interactions with a reasonably high accuracy, as long as no surface ordering takes place, i.e., when the surface potential is weak. Monomer distributions are compared in Figure 10, at a surface amplitude of $A_w = 0.4$. Again, the functional does predict a somewhat too low-density maximum, but the deviation is acceptable. A perhaps even better agreement is obtained for the osmotic pressure, which indeed is more relevant to the findings in this work. A comparison is given in Figure 11.

Conditions under which surface ordering of rods does occur is more relevant to this study, so we shall investigate this case in some more detail. First, we see in Figure 12 how the DFT severely underestimates the height of the first adsorption peak, under identical bulk conditions, when the surface potential is strong ($A_w = 1.25$). To reproduce such a strong adsorption, the surface potential has to be increased substantially, to about $A_w = 1.75$. Surface ordering in simulations can be formally expressed by monitoring various order parameters. However, the mental intepretation of such order parameters are not always transparent and intuitive. We have therefore chosen to present a "configurational snapshot" which, though it is less rigorous, often provide some additional insight. Such a snapshot, displaying a configuration in the left "half-cell" (center of mass $< h/2$), is presented in Figure 13.

The ordering of adsorbed chains is quite evident, as is the random structure of the "free" rods that are not strongly adsorbed.

Finally, we switch focus to the properties we are mainly interested in, namely surface interactions. GCMC data as well

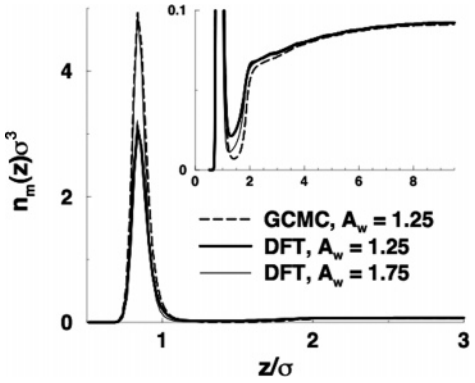

Figure 12. Predicted and simulated monomer density distributions in athermal fluids of rodlike 15-mers between strongly attractive surfaces: $A_w = 1.25$. The surface separation is $h = 19\sigma$. We shall later demonstrate that this system displays smectic-like behavior at the surfaces. The corresponding DFT prediction, at the same bulk pressure, is given by a thick solid line. The thin solid line is the analogous prediction with a stronger surface potential: $A_w = 1.75$. The inset focuses on the low-density regime.

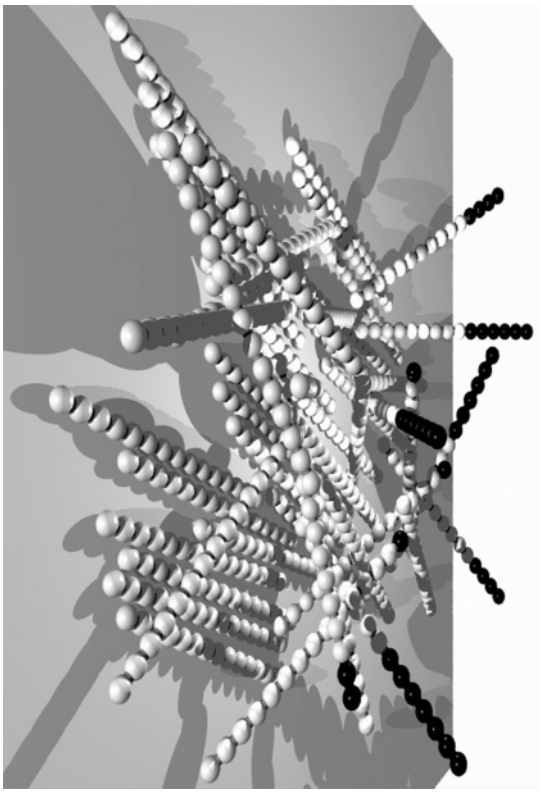

Figure 13. A "snapshot" of a configuration in an GCMC simulation, with $A_w = 1.25$ and at $h = 19\sigma$. Only rods with their center of mass in the left half cell ($z < h/2$) are displayed. Bridging rods contain black monomers, for which $z > h/2$. It should be noted that the periodic boundary conditions have been removed in order to clarify the picture. This means that the system actually is denser than it appears from this graph.

as DFT predictions of how the osmotic pressure varies with surface separation are provided in Figure 14. The overall behavior of the simulated force curve is remarkably well reproduced by the DFT. The reason is that the surface interactions are governed by the free rods or more specifically by the depletion of these rods. Free rods do not display any ordering in the x, y dimensions, and it is therefore not surprising that the DFT predictions of surface forces are accurate. It is important to note that the only influence surface ordering has on the surface forces is that it leads to a more complete surface saturation.

CDV

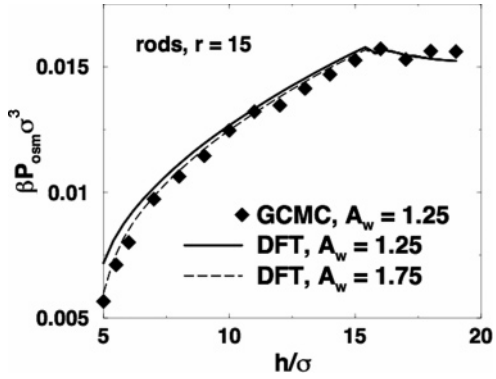

Figure 14. Predicted and simulated osmotic pressure curves in athermal fluids of rodlike 15-mers between strongly attractive surfaces: $A_w = 1.25$. The corresponding DFT prediction, at the same bulk pressure (as estimated by the large separation part of the simulated curve), is given by a thick solid line. The thin solid line is the analogous prediction with a stronger surface potential: $A_w = 1.75$. It is remarkable that an increase of the surface potential by almost 50% has a very small impact on the osmotic pressure curve. Compare also with the results obtained with a weak surface potential, where no surface ordering occurs, i.e., Figure 11.

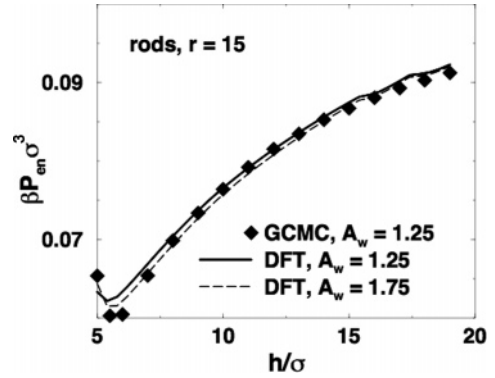

Figure 15. Entropic contribution, P_{en}, to the pressure across the midplane for various separations, as obtained from GCMC simulations and DFT calculations. Bulk conditions are the same as in Figure 14.

This generates a more complete exclusion of free rods from the attractive part of the surface potential and hence to a slightly stronger depletion interaction. That the orientational aspects (in the *x*, *y* directions) of the ordering is *unimportant* in terms of surface interactions is evident from the way in which the simulated osmotic pressure curve is almost quantitatively reproduced by DFT, provided the surface adsorption is increased in order to reproduce the simulated net adsorption (cf. Figure 12). Another manifestation of the small influence of surface ordering on surface interactions is the agreement between the simulated osmotic pressure curves at weak (no surface ordering) and strong (surface ordering) surface potentials (cf. Figures 11 and 14).

It should be pointed out that surface ordering may have a significant influence on the osmotic pressure in other systems where the monomers interact at long range. In those cases, monomer−monomer intrasurface interactions of adsorbed and aligned rods may be relevant (for instance, if the chains are charged).

We have previously stated that the surface interactions in these fluids of rodlike chains are dominated by depletion, i.e., by a net attractive contribution from P_{en}. This corroborated by GCMC results, as illustrated in Figure 15. Again, the agreement between GCMC data and DFT is quite satisfactory.

3. Conclusions

We have investigated the interaction free energy between surfaces immersed in semiflexible and rodlike polymers. The introduction of stiffness to the chain significantly affects the surface interaction. At low to moderate stiffness, one observes the growth of a free energy barrier at intermediate separations, corresponding to the overlap between adsorbed polymer layers. At short separations the interaction is dominated by bridging. As the polymer stiffness approaches the rod limit, however, the free energy barrier begins to diminish due to the fact that the adsorbed layer is more tightly bound to the surface and does not protrude as far into the solution. Instead, one sees the onset of a depletion attraction, which was always present in the case of the more flexible polymers, but which grows significantly as the polymers become stiffer. This depletion attraction dominates across a wide range of the surface interaction. At short surface separations, however, the adsorption layers overlap and the monomer density between the surfaces increases, but the separation is small enough so that bridging will dominate the total interaction. The onset of rodlike behavior depends on the density of polymers in solution. The higher is the density, the closer a semiflexible polymer solution will mimic rods. This is due to the fact that adsorption will be approach saturation (and thus become more that of rods) as the polymer density increases. It is surprising, however, that at low density polymers whose persistence length is comparable to the chain length give rise to surface interactions which are very different to those of rods. This "slow" approach to rodlike behavior is further illustrated by our ideal polymer calculations, which show qualitatively different surface interactions between rods and semiflexible polymers with a persistence length approximately twice the length of the chain. This observation suggests that polymers, even if they are very stiff, almost never can be reliably modeled as rods or cylinders. For instance, it appears unlikely that an unfolded DNA molecule has adsorption characteristics that are even remotely similar to that of a corresponding cylinder. Finally, we have shown that, in the absence of long-ranged monomer−monomer interactions, the occurrence of local ordering at the surfaces have little effect on surface forces. The surface interactions are dominated by the depletion of free (and randomly oriented) chains, which are expelled from the almost completely saturated surfaces.

References and Notes

(1) Forsman, J.; Woodward, C. E., *Macromolecules* **2006**, *39*, 1261.
(2) Flory, P.; Abe, A. *Macromolecules* **1978**, *11*, 1119.
(3) Flory, P. *Macromolecules* **1978**, *11*, 1138.
(4) Bianchi, E.; Ciferri, A.; Conio, G.; Marsano, E.; Tealdi, A. *Macromolecules* **1984**, *17*, 1526.
(5) Lin, K.; Crocker, C.; Zeri, A. C.; Yodh, A. G. *Phys. Rev. Lett.* **2001**, *87*, 088301.
(6) Buitenhuis, J.; Donselaar, L. N.; Buining, P. A.; Stroobants, A.; Lekkerkerker, H. N. W. *J. Colloid Interface Sci.* **1995**, *175*, 46.
(7) Mao, Y.; Bladon, P.; Lekkerkerker, H. N. W.; Cates, M. E. *Mol. Phys.* **1997**, *92*, 151.
(8) Koenderink, G. H.; Vliegenhart, G. A.; Kluijtmans, G. J. M.; van Blaaderen, A.; Philipse, A. P.; Lekkerkerker, H. N. W. *Langmuir* **1999**, *15*, 4693.
(9) Vliegenhart, G. A.; Lekkerkerker, H. N. W. *J. Chem. Phys.* **1999**, *111*, 4153.
(10) Helden, L.; Roth, R.; Koenderink, G. H.; Leiderer, P.; Bechinger, C. *Phys. Rev. Lett.* **2003**, *90*, 048301.
(11) Roth, R. *J. Phys.: Condens. Matter* **2003**, *15*, S277.
(12) Lau, A. W. C.; Lin, K.; Yodh, A. G. *Phys. Rev. E.* **2002**, *66*, 020401.
(13) Very rigid long chains would require extremely large values of the stiffness parameter, which may lead to numerical problems for the CPU, i.e., underflow or overflow errors.
(14) Forsman, J.; Woodward, C. E.; Freasier, B. C. *J. Chem. Phys.* **2002**, *117*, 1915.

(15) Forsman, J.; Woodward, C. E.; Freasier, B. C. *J. Chem. Phys.* **2003**, *118*, 7672.
(16) Forsman, J.; Woodward, C. E. *Phys. Rev. Lett.* **2005**, *94*, 118301.
(17) Woodward, C. E. *J. Chem. Phys.* **1991**, *94*, 3183.
(18) Forsman, J.; Woodward, C. E. *J. Chem. Phys.* **2003**, *119*, 1889.
(19) McMillan, W. G.; Mayer, J. E. *J. Chem. Phys.* **1945**, *13*, 276.
(20) Scheutjens, J. M. H. M.; Fleer, G. J. *Macromolecules* **1985**, *18*, 1882.
(21) Woodward, C. E.; Forsman, J. *Macromolecules* **2004**, *37*, 7034.
(22) Müller, M.; Paul, W. *J. Chem. Phys.* **1994**, *100*, 719.
(23) Svensson, B.; Woodward, C. E. *J. Chem. Phys.* **1994**, *100*, 4575.
(24) Wilding, N. B.; Müller, M. *J. Chem. Phys.* **1994**, *101*, 4324.
(25) Escobedo, F. A.; Suen, J. K. C. *J. Chem. Phys.* **1995**, *103*, 2703.
(26) Escobedo, F. A.; de Pablo, J. J. *J. Chem. Phys.* **1996**, *105*, 4391.
(27) Forsman, J.; Woodward, C. E. *Mol. Simul.* **1997**, *19*, 85.
(28) Czezowski, A. Thesis, ADFA, Canberra, 2001.
(29) Fenwick, M. K.; Escobedo, F. A. *J. Chem. Phys.* **2004**, *120*, 3066.
(30) Forsman, J.; Broukhno, A.; Jönsson, B.; Åkesson, T. *J. Chem. Phys.* **2004**, *120*, 413.
(31) Metropolis, N. A.; Rosenbluth, A. W.; Rosenbluth, M. N.; Teller, A.; Teller, E. *J. Chem. Phys.* **1953**, *21*, 1087.

MA052472+